

# Exploring Kinematic Bifurcations and Hinge Compliance for In-Hand Manipulation: How Could Thick-Panel Origami Contribute?

Chenying Liu, Liang He, Sihan Wang, Albert Williams, Zhong You,\* and Perla Maiolino\*

Origami-inspired mechanisms have found significant applications in end effector design. So far, the exploration of thick-panel origami has been relatively limited, but it is worth noting that the incorporation of rigid thick panels can introduce unique mechanical properties, showcasing great potential in addressing manipulation challenges. Our previous work has developed a gripper from thick-panel waterbomb origami, which can pick up a variety of daily objects. Based on the same prototype, this article extends the gripper's function from grasping to in-hand manipulation, which is attributed to the kinematic bifurcations and compliance of thick-panel origami. A kinematic study is carried out to investigate the gripper's bifurcated motion modes. The hinge compliance is also taken into account to enhance the gripper's motion dexterity. Theoretical analysis and experiments are conducted to demonstrate both features, thereby paving the foundation for achieving dexterous motions with a simplified control strategy. Aided by a differential mechanism, the gripper can effectively interact with objects with the actuation inputs from only two motors. Objects including balls, cuboids, and cones are explored for in-hand manipulation under different motion modes, showing varied trajectories. With the integration of tactile sensors at the fingertips, we have also revealed the gripper's potential for classification tasks.

and grippers, to replicate these functions.<sup>[2,3]</sup> In general, robotic hands are often engineered with multiple fingers to emulate the intricacy and precision of human hand articulations.<sup>[4,5]</sup> One example is the Shadow Dexterous Hand, which possesses 20 actuated degrees of freedom (DoFs) for grasping and manipulation tasks.<sup>[6,7]</sup> Its soft material counterpart, such as the robotics and biology laboratory Hand 3, has 16 independent degrees of actuation for 33 grasp postures.<sup>[8]</sup> Similar five-fingered hands have been developed and well-studied.<sup>[9–12]</sup> While these designs offer enhanced dexterity to mimic human hand movements, their high DoFs also necessitate complex control strategies.<sup>[7]</sup> Additionally, the increased number of DoFs can lead to reduced robustness.<sup>[13]</sup>

In this respect, researchers have explored various approaches to simplify the design of end effectors while preserving their functions to the largest extent. One intuitive approach is to develop end effectors with a reduced number of fingers such as the shape deposition manufacturing (SDM)

Hand<sup>[14]</sup> and the grasp-reposition-reorient (GR2) gripper.<sup>[15]</sup> The former is a four-finger design with compliant materials, controlled by a single motor for adaptable grasping. The latter has two fingers with elastic joints. Each finger, controlled by a servomotor, contributes to object grasping and manipulation on a 2D plane.

It should be noted that grasping and in-hand manipulation are two distinctive functions. Manipulation occurs when an end effector applies forces to purposefully change the state of a grasped object, which is more than just holding it.<sup>[16]</sup> More specifically, a successful grasp could not guarantee that the end effector can manipulate objects, where additional motions are often required. Hence, due to a lack of motion dexterity, many grippers, such as the SDM Hand and a three-finger gripper,<sup>[14,17]</sup> are not suitable for manipulation tasks.


To address the challenge, a significant interest emerges in mechanically reconfigurable grippers to achieve dexterous motions for in-hand manipulation. Fingers with adjustable lengths or stiffness are used to expand the gripper's motion range and generate multiple grasping modes.<sup>[18,19]</sup> The arrangement of finger positions has also been proven to impact the manipulation capability.<sup>[20]</sup> Consequently, a reconfigurable palm has been introduced, as demonstrated by the reconfigurable underactuated constant-tendon hand (RUTH) gripper.<sup>[21]</sup> Made from a 5R planar linkage, the palm

## 1. Introduction

The adaptability and versatility of human hands enable grasping and in-hand manipulation as daily tasks.<sup>[1]</sup> Significant efforts have been devoted to developing end effectors, i.e., robotic hands

C. Liu, L. He, S. Wang, A. Williams, Z. You, P. Maiolino  
 Department of Engineering Science  
 University of Oxford  
 Oxford OX1 3PJ, UK  
 E-mail: zhong.you@eng.ox.ac.uk; perla.maiolino@eng.ox.ac.uk

P. Maiolino  
 Department of Mechanical, Energy, Management and Transport  
 Engineering - DIME  
 University of Genoa  
 16143 Genoa, Italy

 The ORCID identification number(s) for the author(s) of this article can be found under <https://doi.org/10.1002/aisy.202300691>.

© 2024 The Authors. Advanced Intelligent Systems published by Wiley-VCH GmbH. This is an open access article under the terms of the Creative Commons Attribution License, which permits use, distribution and reproduction in any medium, provided the original work is properly cited.

DOI: 10.1002/aisy.202300691

can shift finger positions to facilitate interaction with objects. Moreover, the material phase transition has been employed to attain dexterous manipulation with two actuation inputs.<sup>[22]</sup> These grippers have achieved manipulation tasks in a 3D space with a smaller number of actuators, while it should be noted that these grippers often come with intricate designs.

So far, it has remained a challenge to incorporate in-hand manipulation and grasping into a simplified gripper design, especially when only a small number of control inputs are permitted. To resolve the issue, we have drawn inspiration from origami, whose creased structure has already shown value in gripper design and the wider robotics community, due to its innate compliance, simplicity of modeling, and ease of fabrication.<sup>[23]</sup>

In contrast to most research solely based on thin sheets of origami that are prone to fatigue, our previous work has demonstrated a four-finger gripper developed from an assembly of thick-panel waterbomb origami.<sup>[24,25]</sup> The use of rigid thick panels offers enhanced mechanical coupling compared to zero-thickness ones and thus enables a single-DoF grasping motion. The gripper can be easily 3D-printed and pick up a range of daily objects under the control of only one motor. In this article, we extend the gripper's function to in-hand manipulation with minimal actuation inputs. To achieve this, we leverage two properties of thick-panel origami, namely kinematic bifurcations and compliance. Specifically, the bifurcations allow the gripper to alternate among different motion paths at a certain state without increasing the overall mobility. The compliance not only contributes to motion switches outside bifurcation states but also enables the gripper fingers to finely tune their positions, thereby interacting with grasped objects even if the single-DoF movements of fingers are blocked in theory.

A further-developed gripper platform is to be presented. In addition to the grasping motion, the gripper's kinematic bifurcations are investigated, leading to other motion types. Additionally, to analyze the gripper's compliance, a kinematic model has been proposed considering hinge widths, which allows motion switches at non-bifurcations. Following this, a tendon–pulley-based differential mechanism has been proposed for the overall actuation, so that the gripper can achieve eight kinematic modes and infinite transitions using only two motors. The bifurcations and compliance are experimentally validated. By exploiting the two features,

the gripper platform successfully demonstrates in-hand manipulation of balls, cuboids, and cones, under a rather simplified control strategy. The gripper's function is further unlocked by integrating four tactile sensors at its fingertips, leading to a promising potential in object classification. Limitations and future research avenues are discussed at the end.

## 2. Materials and Methods

### 2.1. Bifurcated Paths of a Single Finger and Its Actuation

The origami pattern and computer-aided design (CAD) model of the gripper are shown in **Figure 1**. The red dashed line highlights finger 1 ( $F_1$ ), which is modeled as a 6R Bricard linkage.<sup>[24]</sup> The finger's kinematic behaviors are analyzed via the loop closure equation, yielding four motion paths as detailed in Equation (1)–(4).

Path 1

$$\tan \frac{\omega_1}{2} = \frac{\sqrt{2}}{2} \tan \frac{\omega_2}{2}, \quad \omega_2 = \omega_3 = \omega, \quad 0 \leq \omega \leq \pi \quad (1)$$

Path 2

$$\omega_1 = \omega_2 = 0, \quad \omega_3 = \omega, \quad 0 \leq \omega \leq \pi \quad (2)$$

Path 3

$$\omega_1 = \omega_3 = 0, \quad \omega_2 = \omega, \quad 0 \leq \omega \leq \pi \quad (3)$$

Path 4

$$\omega_2 = \omega_3 = 0, \quad 0 \leq \omega_1 \leq \pi \quad (4)$$

where  $\omega_i$  is a dihedral angle as marked in **Figure 2a** and each path is plotted in **Figure 2b**.

The finger has a single mobility, with a sudden increase in its DoFs at its bifurcation point, i.e., the unfolded state. This characteristic not only enables the finger to be controlled in each motion path with ease but also allows for the possibility to transit between multiple configurations. With the tendon channel design, i.e.,  $T_1$  depicted in **Figure 1**, paths 1–3 of a finger can be achieved by pulling tendons separately or in combination. Take  $F_1$  as an example. Pulling  $T_4$  or  $T_1$  will lead the finger into

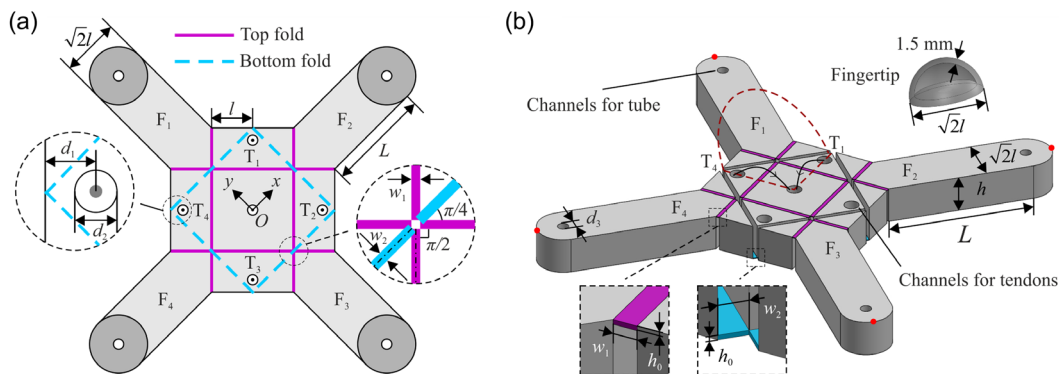


**Figure 1.** Gripper design. a) Top view of the gripper with a parameterized fold pattern. The gripper consists of four waterbomb units assembled at the center. The  $z$  direction points out of the paper. b) CAD model of the gripper backbone for 3D printing. Each fingertip is designed hollow inside so that it can work as a pneumatic sensor.<sup>[31]</sup> Tendons associated with  $F_1$ , i.e.,  $T_1$  and  $T_4$ , are also indicated.

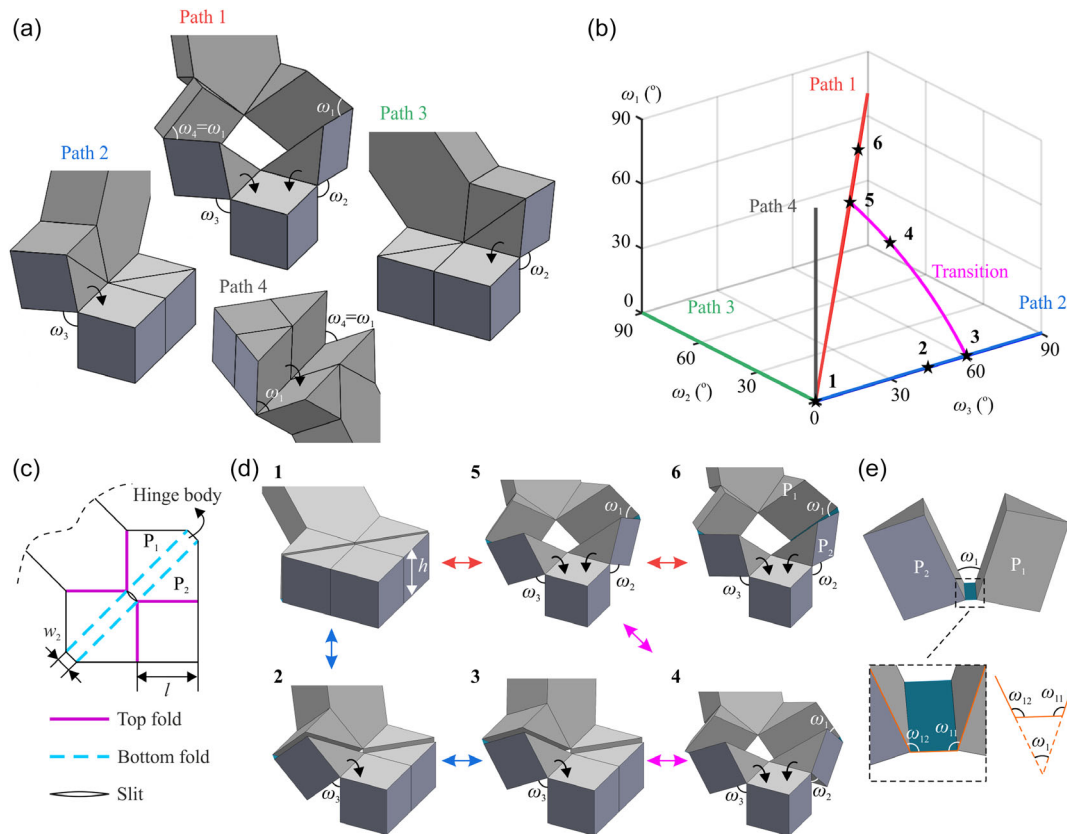


**Figure 2.** Kinematic behaviors of a single finger. a) Four basic configurations when each fold is considered to be the centerline of a hinge, as exemplified by the dash-dot lines in Figure 1a. b) Kinematic paths of a finger. The transition between paths 1 and 3 is omitted as it is essentially symmetric to the one between paths 1 and 2. c) Fold pattern of a finger with hinge width taken into account. d) Selected configurations of a finger when hinge widths are considered in the kinematic model. e) Dihedral angles among the hinge body and the thick panels.

its path 2 or path 3 shown in Figure 2a, respectively. When  $T_1$  and  $T_4$  are pulled together at the flat state, the finger switches to its path 1. Path 4 is disabled, as the current tendon arrangement cannot achieve it. The folds are designed to be elastic, so that  $F_1$  can return to its flat configuration once the tendons are released.

While only  $F_1$  and its associated two tendon channels are taken as an example, the actuation principle can be extended to the entire gripper backbone by symmetry. Notably, the gripper backbone has four fingers, which are mechanically coupled via shared folds and panels. Thus, pulling  $T_1$  or  $T_4$  will also cause movements in fingers that are adjacent to  $F_1$ . For example, simply pulling  $T_4$  will also activate  $F_4$  in the corresponding motion path, which should be taken into account in the gripper motion analysis.

## 2.2. Hinge Compliance for Dexterous Motions

Paths 1–3 of a single finger are not sufficient for in-hand manipulation. This is because, theoretically, they can only switch among each other at the bifurcation state. The gripper's shape adaptability observed in ref. [25] indicates a certain level of compliance, which has the potential to enable motion switches outside of bifurcations. Hence, this feature is exploited to improve the dexterity of the gripper.

Instead of simulating the material behavior with finite-element modeling, a new kinematic model is proposed to analyze the hinge compliance and how more motions can be obtained from the finger. Figure 2c presents a fold pattern for  $F_1$  where hinge widths are taken into account. Specifically, the bottom folds are replaced by two rigid hinge bodies with width  $w_2$  and thickness of zero. Each hinge body has two revolute connections with its adjacent thick panels. The top folds retain as perfect rotary joints for the simplicity of modeling. Consequently, the finger is modeled as an 8R spatial linkage rather than the previous 6R linkage.

The detailed kinematic analysis of the finger is available in Section S1, Supporting Information. It is discovered that the new model not only has the same paths as the original ones but also possesses a transition mode to switch between different paths at non-bifurcation states, as shown in Figure 2d. Taking the transition between paths 1 and 2 as an example, its kinematic behaviors are derived as follows.

$$\tan \omega_1 = \frac{\sqrt{2}(\sin \omega_2 + \sin \omega_3 - \sin(\omega_2 + \omega_3))}{\cos \omega_2 + \cos \omega_3 - 2 \cos \omega_2 \cos \omega_3 + \sin \omega_2 \sin \omega_3} \quad (5)$$

where  $\omega_3$  is fixed at a certain value, defined as the transition angle. In practice, it refers to a state when the finger is semi-folded in its path 2.

Selected configurations of the new model are marked on the kinematic plots in Figure 2b for comparison, along with the transition path. The finger starts from position 1, the original bifurcation state, and passes along positions 2 and 3 along path 2 until  $\omega_3$  reaches  $60^\circ$ . Keep  $\omega_3$  fixed and let  $\omega_2$  increase from 0. The finger subsequently passes position 4 in the transition path and then reaches position 5 where  $\omega_2 = \omega_3$ . The finger is now in path 1, where  $\omega_2$  and  $\omega_3$  can increase synchronously to get to position 6.

According to Figure 2, it seems that the finger can transit from path 1 to 2 without passing the bifurcation point as long as the bottom hinge width is considered. However, it is also important to examine whether the angles between the hinge body and thick panels, i.e.,  $\omega_{11}$  and  $\omega_{12}$  as illustrated in Figure 2e, can exist in reality without physical interference. Given the analysis in Section S1, Supporting Information,  $\omega_{11}$  and  $\omega_{12}$  are obtained as

$$\tan \frac{\omega_{11}}{2} = \frac{-B_{11} + \sqrt{B_{11}^2 - 4A_{11}C_{11}}}{2A_{11}}, \quad \omega_{12} = \omega_1 + 180^\circ - \omega_{11}$$

where

$$A_{11} = -\left(1 + \frac{w_2}{h}\right)(\sin \omega_3 + \sin \omega_2 \cos \omega_3) + \sin \omega_2 + \cos \omega_2 \sin \omega_3$$

$$B_{11} = \sqrt{2} \frac{w_2}{h} (\sin \omega_2 \sin \omega_3 + \cos \omega_2 - \cos \omega_3)$$

$$C_{11} = -\left(1 - \frac{w_2}{h}\right)(\sin \omega_3 + \sin \omega_2 \cos \omega_3) + \sin \omega_2 + \cos \omega_2 \sin \omega_3 \quad (6)$$

where  $\omega_{11}$  and  $\omega_{12}$  are between  $0^\circ$  and  $260^\circ$  to avoid collisions between the hinge body and thick panels.

It is found that  $\omega_{12}$  is the key constraint when  $w_2/h$  varies. Figure 3 illustrates the relationship between  $\omega_{12}$  and  $\omega_2$  in the transition path at multiple values of  $w_2/h$  and  $\omega_3$ . Take Figure 3b as an example where  $\omega_3 = 60^\circ$ . When  $w_2/h = 0.04$ ,  $\omega_{12}$  drops to 0 as illustrated in Figure 3d and  $\omega_2$  is no more than  $7.5^\circ$ . The result indicates that the finger cannot move from position 3 to 5 along the transition path, as  $\omega_2$  cannot reach the same value as  $\omega_3$ . When  $w_2/h$  increases gradually and passes a threshold value of 0.1082,  $\omega_{12}$  would increase before dropping to zero and  $\omega_2$  is then able to reach  $60^\circ$ , the same value as the transition angle. Hence, a wider hinge means higher compliance, as the gripper can more easily switch from one path to the other in

the semi-folded configuration. However, if the hinge becomes too wide, the kinematic model cannot hold as the hinge is soft and cannot be taken as a rigid body. Comparing all three graphs in Figure 3, it is also noticed that the threshold value increases with the transition angle. This means when the gripper is closer to its bifurcation point, the transition is easier to take place.

In terms of actuation, the tendon arrangement in Figure 1 is sufficient to support the motion switch by controlling  $\omega_2$  and  $\omega_3$  separately. Specifically,  $T_4$  can be pulled first so that the finger moves along path 2. The tension on  $T_4$  is adjusted so that  $\omega_3$  is kept at a certain value, e.g.,  $60^\circ$ .  $T_1$  is activated thereafter and the finger transits via position 4 until  $\omega_2$  also reaches  $60^\circ$ , at which point the finger is in path 1. By choosing different transition angles, the finger can generate infinite transition paths outside of bifurcations.

### 2.3. Motion Mode Analysis of the Gripper

Each tendon channel can have multiple tendon outputs. There are four tendon channels in total on the gripper backbone, and hence, their output tendon combinations can generate diverse modes on the gripper. With an exhaustive permutation of all possible tendon combinations, it is found that the gripper's modes can be categorized into five basic types as shown in Table 1 and a variety of transitions in between. Paths 2 and 3 of a single finger are conceived symmetric, and thus, they are not distinguished in the analysis. The endpoint of each finger, marked by a red dot in Figure 1b, is used to represent its motion trajectory. To have a clearer picture of how the gripper behaves, the five motion types are illustrated in Figure 4a–e, where symmetric motions are also omitted.

In Table 1,  $(x_{ij}, y_{ij}, z_{ij})$  represents the coordinates of finger  $j$  under motion type  $i$ . According to the finger kinematics in Equation (1)–(4), the unknown coordinates,  $(x_{11}, y_{11}, z_{11})$  and  $(x_{21}, y_{21}, z_{21})$  from Table 1 are given as

$$x_{11} = -\left(\frac{1}{2}L + \frac{\sqrt{2}}{2}l + \frac{\sqrt{2}}{4}w_1 + \frac{1}{2}w_2\right)(1 - \cos \omega)$$

$$y_{11} = \sqrt{2} + \frac{\sqrt{2}}{2}w_1 + \left(\frac{1}{2}L + \frac{\sqrt{2}}{2}l + \frac{\sqrt{2}}{4}w_1 + \frac{1}{2}w_2\right)(1 + \cos \omega) \quad (7)$$

$$z_{11} = \left(\frac{\sqrt{2}}{2}L + l + \frac{1}{2}w_1 + \frac{\sqrt{2}}{2}w_2\right) \sin \omega$$

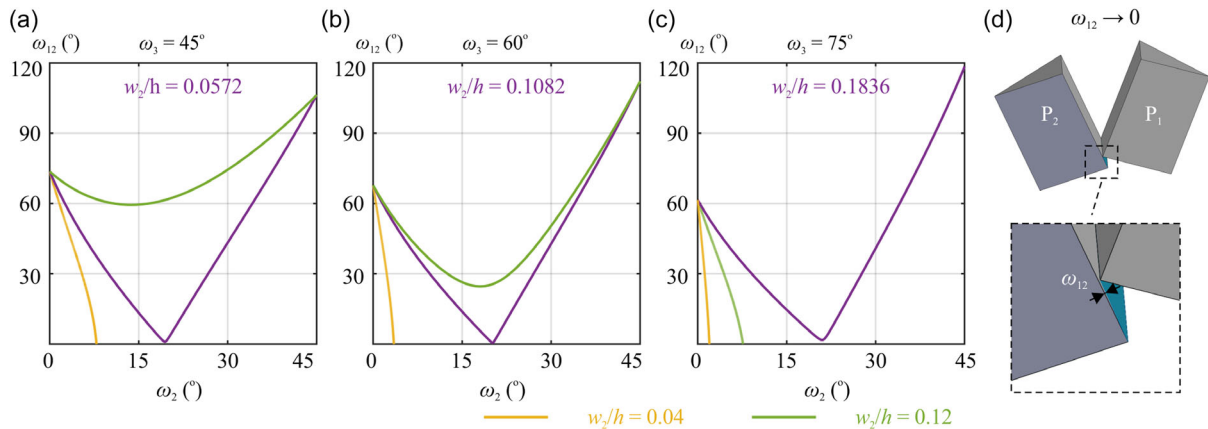


**Figure 3.** The relationship between  $\omega_{12}$  and  $\omega_2$  when the transition angle  $\omega_3$  is fixed at a)  $45^\circ$ , b)  $60^\circ$ , and c)  $75^\circ$ . The threshold value of  $w_2/h$  is indicated. d)  $\omega_{12}$  reaches its lowest extreme.



**Table 1.** Gripper motion type, relevant tendon arrangements, and kinematic behaviors.

Type	Active tendon	Active finger	Finger motion	Path	Mobility	Alternatives
1	$T_1$	Finger 1	$x_{11}, y_{11}, z_{11}$	2 or 3	1 DoF	$T_2$ or $T_3$ or $T_4$
		Finger 2	$x_{12} = y_{11}, y_{12} = x_{11}, z_{12} = z_{11}$	2 or 3		
2	$T_1 T_4$	Finger 1	$x_{21}, y_{21}, z_{21}$	1	1 DoF	$T_1 T_2$ or $T_2 T_3$ or $T_3 T_4$
		Finger 2	$x_{22} = y_{11}, y_{22} = x_{11}, z_{22} = z_{11}$	2 or 3		
		Finger 4	$x_{24} = -y_{11}, y_{24} = x_{11}, z_{24} = z_{11}$	2 or 3		
3	$T_1 T_3$	Finger 1	$x_{31} = x_{11}, y_{31} = y_{11}, z_{31} = z_{11}$	2 or 3	2 DoFs	$T_2 T_4$
		Finger 2	$x_{32} = y_{11}, y_{32} = x_{11}, z_{32} = z_{11}$	2 or 3		
		Finger 3	$x_{33} = -x_{11}, y_{33} = -y_{11}, z_{33} = z_{11}$	2 or 3		
		Finger 4	$x_{34} = -y_{11}, y_{34} = -x_{11}, z_{34} = z_{11}$	2 or 3		
4	$T_1 T_3 T_4$	Finger 1	$x_{41} = x_{21}, y_{41} = y_{21}, z_{41} = z_{21}$	1	1 DoF	or $T_1 T_2 T_3$ or $T_1 T_2 T_4$ or $T_2 T_3 T_4$
		Finger 2	$x_{42} = y_{11}, y_{42} = x_{11}, z_{42} = z_{11}$	2 or 3		
		Finger 3	$x_{43} = -x_{11}, y_{43} = -y_{11}, z_{43} = z_{11}$	2 or 3		
		Finger 4	$x_{44} = -y_{21}, y_{44} = x_{21}, z_{44} = z_{21}$	1		
5	$T_1 T_2 T_3 T_4$	Finger 1	$x_{51} = x_{21}, y_{51} = y_{21}, z_{51} = z_{21}$	1	1 DoF	None
		Finger 2	$x_{52} = y_{21}, y_{52} = x_{21}, z_{52} = z_{21}$	1		
		Finger 3	$x_{53} = x_{21}, y_{53} = -y_{21}, z_{53} = z_{21}$	1		
		Finger 4	$x_{54} = -y_{21}, y_{54} = x_{21}, z_{54} = z_{21}$	1		

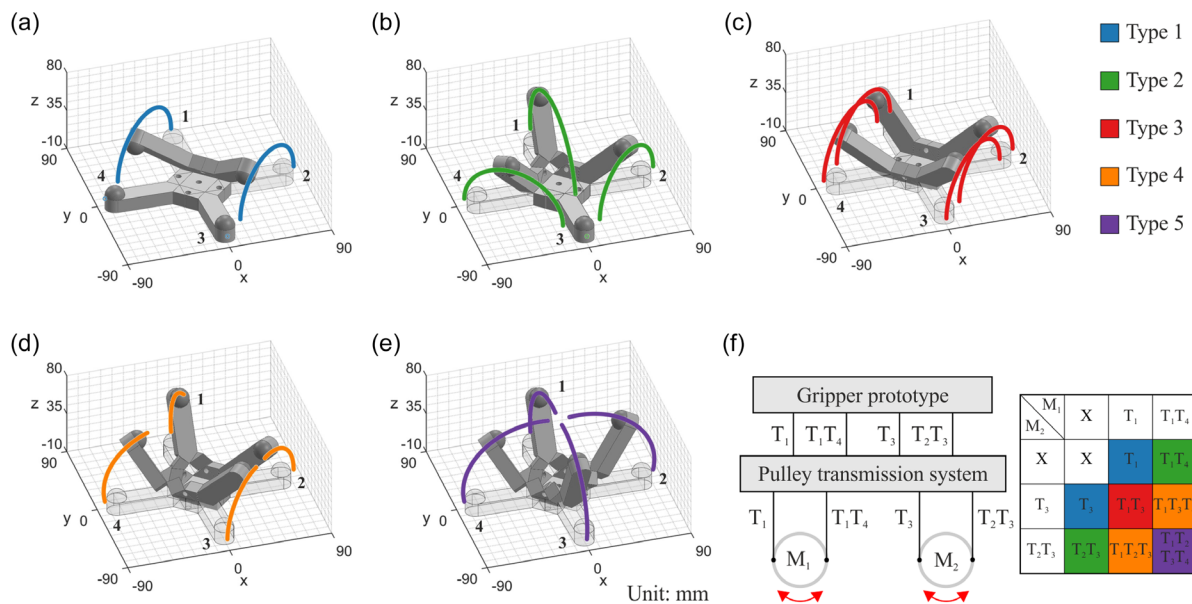


**Figure 4.** The gripper's motion types and differential mechanism for actuation. a–e) Fingertip trajectories of five motion types under the actual fabrication parameters. Note that fingers are numbered for clarity and motion type 5 is the grasping motion examined in ref. [25]. f) A tendon–pulley-based differential mechanism where four sets of tendons are controlled by two motors to achieve eight motion modes. X indicates that the motor is immobile.

$$\begin{aligned}
 x_{21} &= 0 \\
 y_{21} &= \sqrt{2}l + \frac{\sqrt{2}}{2}w_1 + \frac{1}{2}w_2 + h \sin \omega_1 \\
 &\quad + \left( L + \sqrt{2}l + \frac{\sqrt{2}}{2}w_1 + \frac{1}{2}w_2 \right) \cos \omega_1 \\
 z_{21} &= h(1 - \cos \omega_1) + \left( L + \sqrt{2}l + \frac{\sqrt{2}}{2}w_1 + \frac{1}{2}w_2 \right) \sin \omega_1
 \end{aligned} \tag{8}$$

where the relationship between  $\omega$  and  $\omega_1$  is obtained from Equation (1).

The range of  $\omega$  in Equation (7) and (8) varies under different motion types. For motion types 1–3,  $\omega$  ranges from  $0^\circ$  to  $180^\circ$ . For motion types 4 and 5, the range changes to  $[0^\circ, 95^\circ]$  and  $[0^\circ, 125^\circ]$ , respectively. Motion type 3 performs motion type 1 on opposite sides of the gripper, making it the only two-DoF movement of the gripper. All these motions are

switchable at the bifurcation point, i.e., when the gripper is in the flat unfolded state.

In addition to the basic motion types, transitions between some of them at non-bifurcation points are also possible given the hinge compliance analysis. By activating two sets of tendons in sequence, some of the fingers could change their motion paths between path 1 and paths 2 or 3, enhancing the gripper's dexterity on top of the basic motions.

## 2.4. A Differential Mechanism for Minimal Actuators

While most motion types in Table 1 are of single mobility, the bifurcation feature still necessitates the need for a proper actuation system to enable motion switches. The gripper aims to 1) realize all five types; 2) achieve as many transition paths as possible; and 3) employ a minimum number of actuators. Hence, a tendon–pulley-based differential mechanism is proposed in Figure 4f, which allows for the use of only two motors.

Specifically, two motors, i.e.,  $M_1$  and  $M_2$ , are connected with four sets of tendons. The two motors can be activated independently or in combination, with either clockwise (CW) or anticlockwise (ACW) rotation. Each motor's rotation leads to the pulling of one tendon set and the loosening of the other. The pulled tendon set contributes to the gripper's motion. Thus, the permutation of motor combinations gives eight motion modes of the gripper as shown in Figure 4f, where the pulled tendon sets are supposed to operate simultaneously.

**Table 2.** Transitions from one motion to another when the gripper is semi-folded.

Motor in action	Rotation	Initial motion	Added motor	Rotation	Final motion
M1	ACW	Type 1	M2	ACW	Type 3
				CW	Type 4
	CW	Type 2		ACW	Type 4
				CW	Type 5

In addition, the two motors can operate in sequence to enable the transition paths at non-bifurcation states. For all motion types that require the use of both motors, i.e., motion types 3–5, they can be switched from motions using only one motor by activating the other motor. The possibilities are summarized in Table 2. Note that  $M_1$  and  $M_2$  are equivalent. Therefore, we only list cases where  $M_1$  is activated first, followed by which  $M_2$  is added. In Table 2, the finished motion type 3 is a result of the two-DoF motion as stated in Table 1. The finished motion types 4 and 5 are due to hinge compliance.

## 2.5. Fabrication and Experimental Setup

The gripper backbone is 3D-printed. Full fabrication details and experimental procedure are given in Experimental Section. The gripper platform, shown in Figure 5a, is used to demonstrate the basic motion modes and transitions in between. In-hand manipulation of objects will also be explored on this platform. Additionally, the research in ref. [26] has shown that compliance can shape tactile patterns, which can help to further unlock the gripper's potential in object classification, as exemplified by the work in ref. [27]. Hence, the gripper is also actuated as shown in Figure 5b to collect the contact information between fingers and objects. Specifically, four pneumatic sensors are taken as fingertips for tactile data collection. Followed by a series of grasping tasks, the collected data will be analyzed to enhance our understanding of the gripper.

## 3. Results and Discussion

### 3.1. Basic Motion Modes of the Gripper

Figure 6 depicts fingers' experimental positions against the theoretical models. Associated motor states are also indicated. Eight motion modes under five motion types have been demonstrated, a video of which is available in Section S2, Supporting Information. The displacement between each path and its theoretical line is

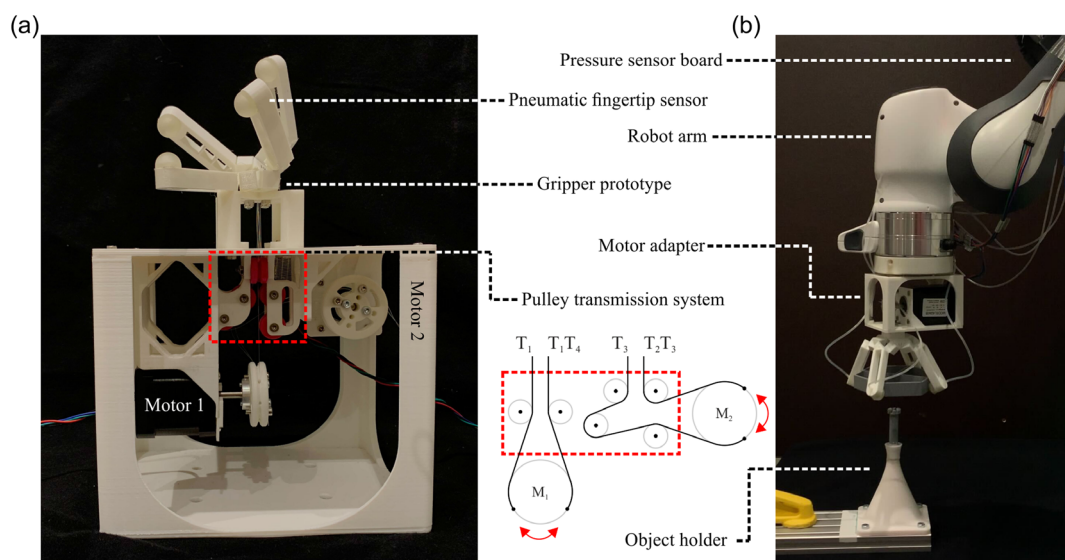


**Figure 5.** Experimental setup. a) Gripper platform with the differential mechanism. A pulley transmission system was used to guide the tendons. b) The gripper is mounted on a robotic arm for grasping tasks and tactile data collection.

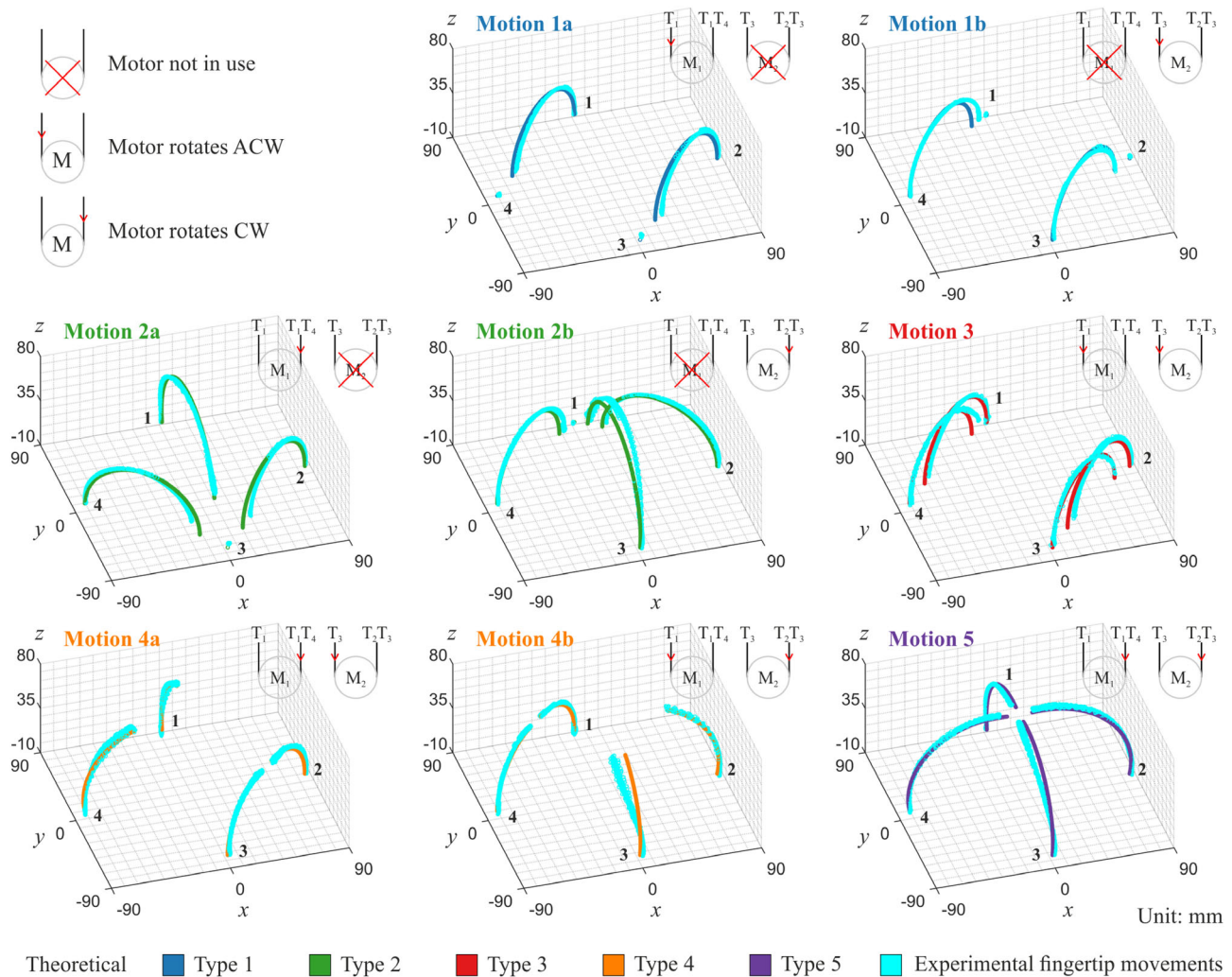


**Figure 6.** Comparison of experimental and theoretical motion paths of the gripper when only one motor is needed or two motors are operated simultaneously. Fingers are numbered for clarity.

quantified. Specifically, for a finger at a certain position, the error is calculated as the shortest distance between the measured position and the theoretical line. The root-mean-square error (RMSE) is the standard deviation of all the errors. ME represents the maximum error in the path. The RMSE and ME of each finger under different modes are summarized in Table 3.

The RMSE in all motion modes ranges from 0.5 to 3.5 mm, indicating relatively good alignment with the theoretical models. The ME varies, with a minimum of 1.92 mm for finger 1 under motion 1b and a maximum of 12.32 mm for finger 3 under motion 4b. This suggests that under some motion types, a finger's actual motion can have a quite big discrepancy from its theoretical trajectory. The difference could be attributed to the gripper compliance and uneven force distribution on tendons.

### 3.2. Motion Switch at Non-Bifurcations

Figure 7 shows the experimental transitions from one motion mode to the other when the gripper is in a semi-folded state.

**Table 3.** RMSE and ME of experimental motion paths (unit: mm).

Motion	Finger 1		Finger 2		Finger 3		Finger 4	
	RMSE	ME	RMSE	ME	RMSE	ME	RMSE	ME
1a	1.68	4.34	2.60	6.46	3.32	5.18	1.44	2.87
1b	1.36	1.92	1.57	2.74	1.92	5.71	2.56	6.87
2a	1.86	5.29	2.44	6.56	3.24	4.24	1.62	4.77
2b	1.51	2.25	1.34	3.05	2.26	7.80	2.06	5.01
3	1.50	3.78	2.18	6.54	1.37	4.49	1.71	6.77
4a	1.70	6.67	1.70	4.06	1.35	2.75	0.94	8.72
4b	1.20	5.28	1.43	3.66	2.26	12.32	1.21	3.24
5	2.35	4.87	1.33	5.29	1.80	6.71	1.18	4.49

The transition phases are highlighted and only exist on some of the fingers. A video of the switching processes is in Section S2, Supporting Information. Such phenomena validate our hypothesis from the hinge compliance analysis.



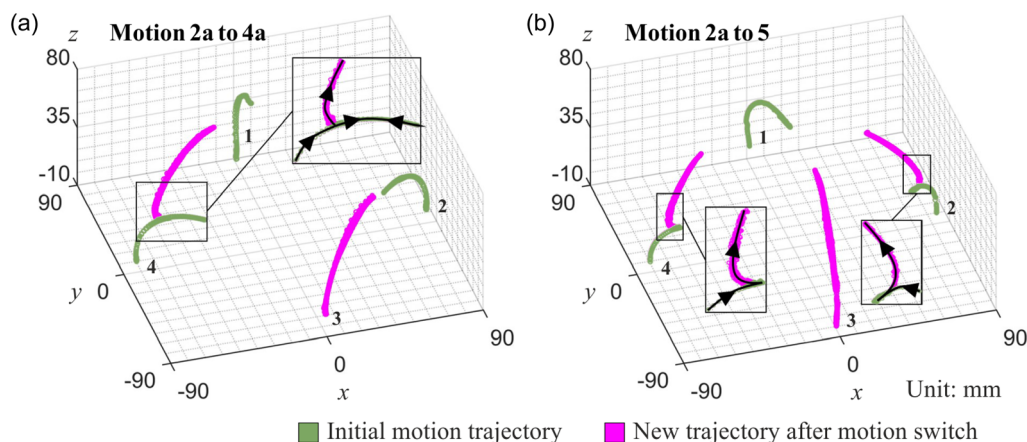


**Figure 7.** Compliant motion switch from a) motion 2a to motion 4a and b) motion 2a to motion 5. The switch process occurs outside of the gripper's bifurcation. Fingers are numbered for clarity.

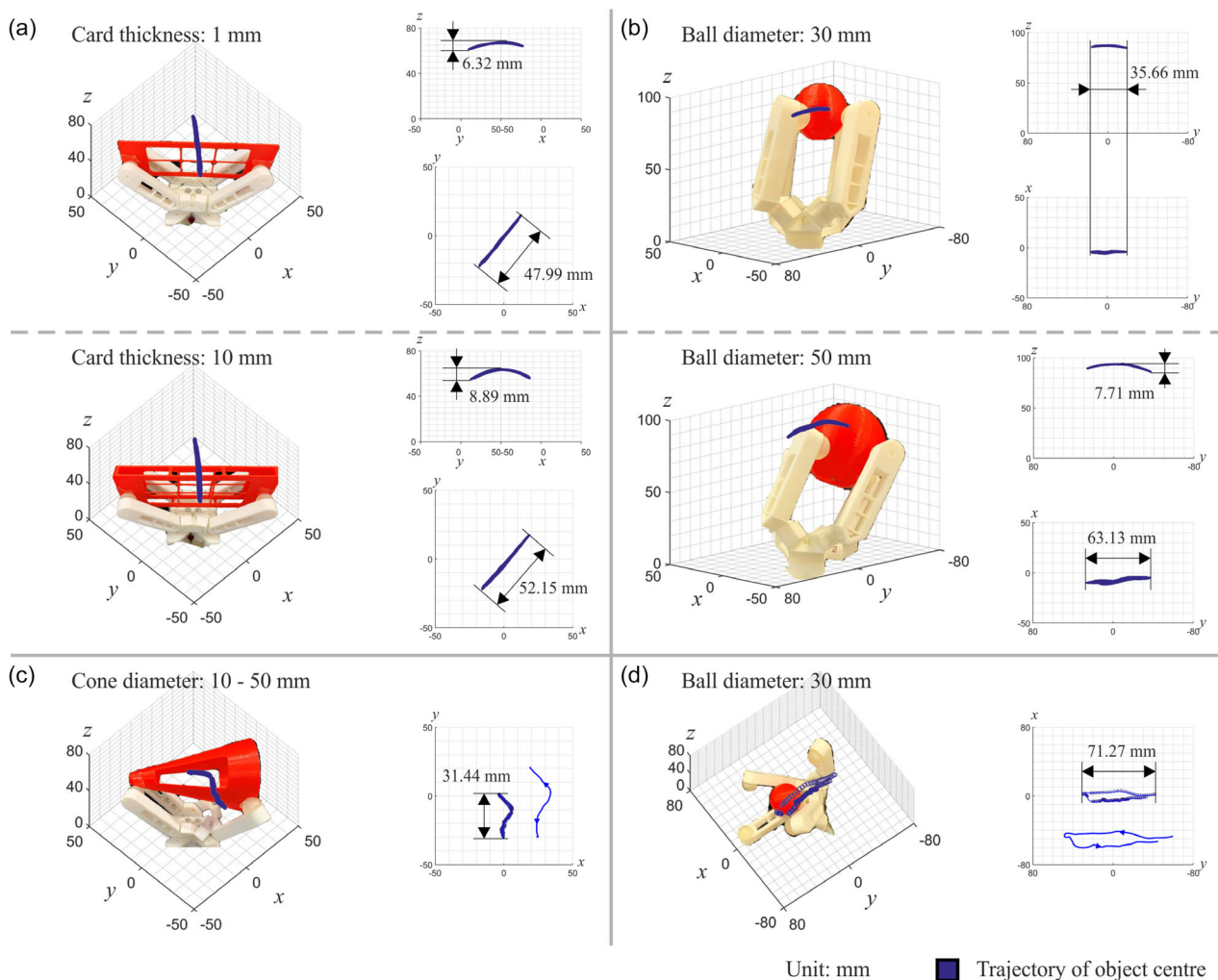


**Figure 8.** In-hand manipulation of objects. a) Cuboid manipulation under motion type 3. Each object's trajectory is roughly an arch whose size varies along with the cuboid thickness. b) Ball manipulation 1 under motion type 5. The smaller ball's trajectory is close to a line while the bigger one still has a curvature. c) Cone manipulation under motion type 4. A complex motion trajectory is obtained. d) Ball manipulation 2 under combined motion types 2 and 5 along their transition paths at non-bifurcations. The ball's motion range is up to 71 mm.



### 3.3. In-Hand Manipulation of Objects

The gripper has demonstrated its capability for in-hand manipulation with only two motors, as shown in **Figure 8**. A video of all manipulation tasks is available in Section S2, Supporting Information.

The in-hand manipulation presented here is a purely exploration task with the open-loop control of two motors. It has been observed that the object motion trajectories vary, depending on the gripper's motion mode as well as the object shape. For instance, as shown in Figure 8a, under motion type 3, the trajectories of both cuboids are approximately an arch, while in Figure 8b, the balls have a more translational movement under

motion type 5. The object size also matters, as the curvatures of these trajectories differ. In addition to translational and rotational movements, complex trajectories can be achieved, as shown in Figure 8c, where a cone is manipulated under motion type 4.

In most manipulation tasks, constant contact between fingertips and the object is a prerequisite. However, manipulation tasks can also be done in another way. As demonstrated in Figure 8d, the gripper's finger bases also interact with the ball and continuous fingertip contact is not needed. The ball has reached a relatively wide motion range of up to 71 mm, roughly the distance between the gripper center and one of its finger ends.

In summary, the basic motion modes have played an important role in object manipulation. For instance, cuboid

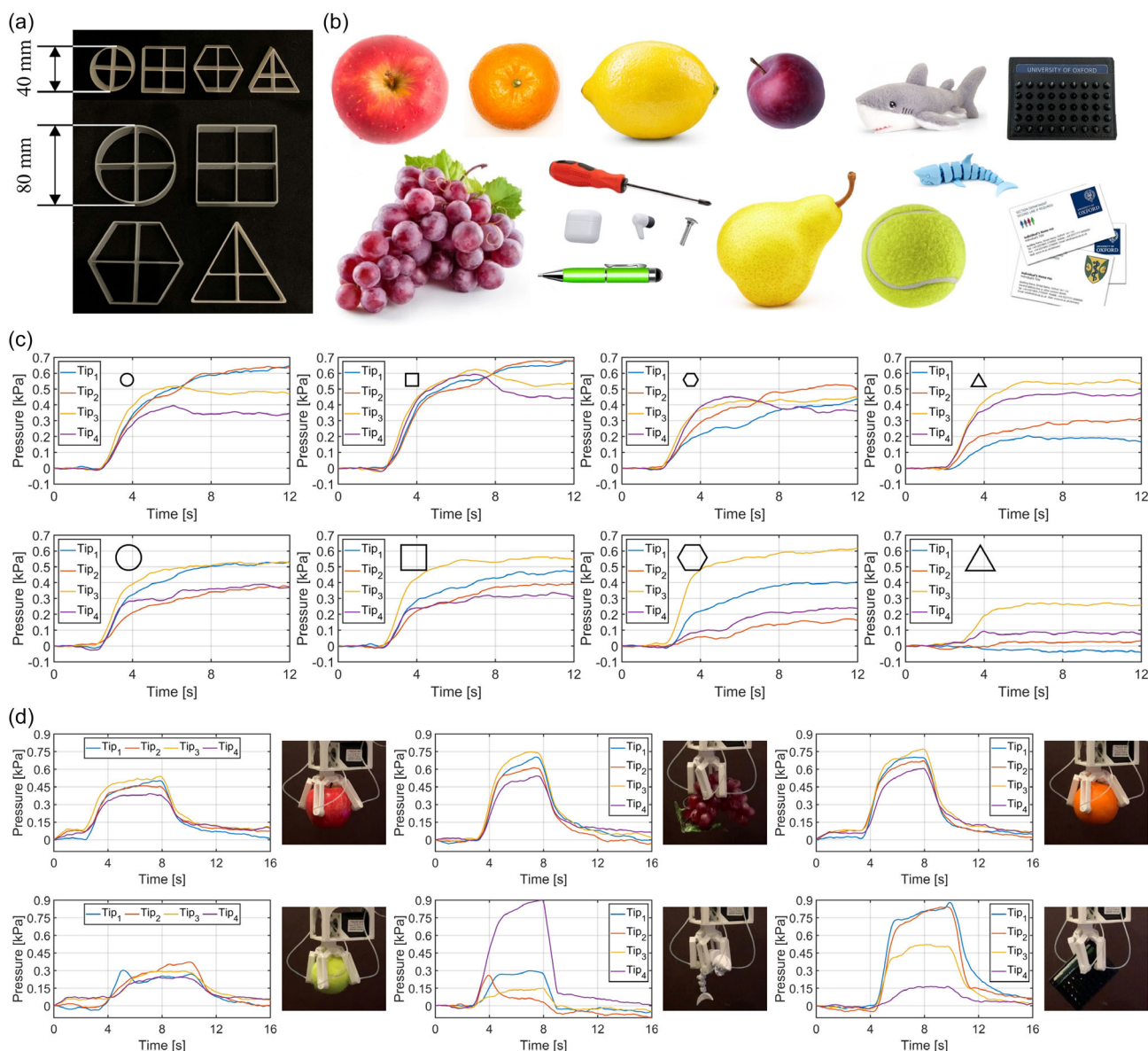


**Figure 9.** Grasping experiments and tactile data. a) Standardized objects with four regular shapes and two sizes. b) Daily objects for grasping, which include an apple, an orange, a lemon, a plum, a fluffy shark toy (toy 1), a cardholder with rivets, grapes, a screwdriver, an earbud box, an earbud, a screw, a pen, a pear, a 3D-printed shark toy (toy 2), a tennis ball, and business cards. The cards and cardholders are grasped from two orientations. c) Tactile data on standardized objects, whose shapes and sizes are also indicated. d) Selected tactile data on daily objects and grasping images.

**Table 4.** Property prediction of daily objects.

Object	Apple	Grape	Lemon	Orange	Pear	Plum	Toy 1	Card 1	Cardholder 1
Size	B	S	B	S (B)	S (B)	S	S	B <sup>a)</sup> (S)	S
Shape	C	S (C)	T (H)	S (C)	S (C)	T (C)	T	H <sup>b)</sup> (S)	C (S)
Symmetry	H	H	L	H	H	L (H)	L	L <sup>c)</sup> (H)	H
Object	Earphone	Box	Ball	Pen	Screw	Screwdriver	Toy 2	Card 2	Cardholder 2
Size	S	B <sup>d)</sup> (S)	S (B)	S	S	B (S)	S	S	S
Shape	H	C <sup>e)</sup> (S)	H <sup>f)</sup> (C)	T (H)	H	H	T	C (S)	T (S)
Symmetry	L	H	L (H)	L	L	L	L	H	L (H)

<sup>a)</sup>Refers to 72% B and 28% S; <sup>b)</sup>Refers to 16% C, 11% S, 41% H, 32% T; <sup>c)</sup>Refers to 27% H and 73% L; <sup>d)</sup>Refers to 26% S and 74% B; <sup>e)</sup>Refers to 74% C and 26% S; <sup>f)</sup>Refers to 81% H and 19% T.

Only the highest proportion is taken as the prediction result. It should also be noted that the actual properties are based on the grasped part of an object, rather than its overall shape, size, or symmetry.

manipulation, ball manipulation 1, and cone manipulation exploit a certain motion type which best suits the object shape. Forces can then be exerted on the object to change its position. The successful in-hand manipulation is also attributed to the gripper's compliance. Most of the gripper's motion types are single DoF. In theory, their movements will be blocked when touching an object. Compliance could allow the fingers to continuously move the object without damaging it. In addition, compliance would enable motion transitions at non-bifurcation states, which has been used in ball manipulation 2.

### 3.4. Analysis of Tactile Data

The gripper was actuated under motion type 5 to grasp a set of standardized objects with regular shapes as well as daily objects, as shown in **Figure 9a,b**. The pressure changes in fingertips are normalized as tactile data, some of which are plotted across the timescale as shown in **Figure 9c,d**. The preliminary data processing steps and all results are available in Section S3, Supporting Information.

For each standardized object, the tactile data are labeled by their size, shape, and symmetry about the fingertips during part of the stable grasping period, e.g., 10–12 s in **Figure 9c** when the gripper can hold the object without other supports. The size of an object is marked as small (S) or big (B) for those with a side length of 40 or 80 mm. For the object shape, C, S, H, and T refer to circle, square, hexagon, and triangle, respectively. For symmetry about the finger arrangement, the circle and square are regarded with high (H) symmetry, leaving the hexagon and triangle with low (L) symmetry. The tactile data of four fingertips and their labels were taken as the input in the Classification Learner app of MATLAB workspace. A k-nearest neighbors classifier was trained.

The classifier was then exported as a model to predict the properties of daily objects, for which 100 sets of tactile data during the stable grasping period in **Figure 9d** were used as the input. The prediction results are summarized in **Table 4**, where the wrong predictions are followed by the actual properties in the brackets. The prediction accuracy for size, shape, and symmetry is 66.7%, 33.3%, and 77.8%, respectively.

The size and symmetry prediction is more promising than the shape one. However, since we have only used four shapes with a small number of data to train the classifier, many actual shapes of daily objects are not well described. For instance, the contact area between the fingers and the lemon can be better approximated as a rectangle rather than a hexagon, but this was not included in the training model. Extra small objects such as the card whose thickness is close to zero are also difficult to predict. The predictions of the cardholder vary by grasping orientations, which is likely due to the rivets on its surface. Additionally, many wrong predictions occur between squares and circles, which share the same symmetry level. This issue can be addressed by grasping the same object multiple times from different orientations. The overall prediction accuracy can be improved with more tactile data and precise labels.

## 4. Conclusions and Future Work

In this article, an origami-based gripper has been encoded with in-hand manipulation functions, where a simple design, actuation, and control strategy is used. The result challenges the common views in robotics. To be more specific, a single-DoF design was chosen to work as the gripper backbone, which is normally thought to have very limited capability. However, the gripper design has now demonstrated its potential to complete manipulation tasks without an intricate control scheme.

The results are naturally linked to two terms, embodied intelligence and morphological computation. The former refers to intelligence that requires and leverages the properties of a physical body to produce desired behaviors in robots.<sup>[28]</sup> The latter exploits morphological features to develop intelligent bodies to obtain better-performing robots.<sup>[29]</sup> In terms of the gripper, many morphological features have contributed to its "intelligence", i.e., the diverse motion modes for object manipulation under the control of only two motors. In particular, the single-DoF motion paths, the kinematic bifurcations, and the gripper compliance are truly fundamental. Any of these features can be extended to other robotic applications, especially those that require dexterous motions and simplified control.

To improve our understanding of the gripper's physical properties, we also collect fingertip tactile data when grasping objects.

The results and associated analysis indicate that the gripper has the potential to identify objects' size and symmetry via the simplest grasping motion. It is expected that with more training data input and better labels, the tactile patterns can be used for object classification.

Given the aforementioned aspects, future work will be around the following areas. 1) More thick-panel origami designs with low DoFs should be investigated extensively, thereby providing a comprehensive database for more versatile robotic applications. 2) Bifurcations can be used to enhance the system's reconfigurability, i.e., the ability to morph into different configurations. A preliminary kinematic study is already available in ref. [30]. 3) A small hinge has a big influence on the gripper and is the key to yield compliance. It would be beneficial to study how hinges could change the behaviors of other thick-panel origami. 4) More work should be conducted using tactile sensors to enable functions such as object classification and tactile-based control. This will further improve the gripper's embodied intelligence.

## 5. Experimental Section

**Gripper Fabrication and Experimental Setup:** The gripper backbone was 3D-printed using thermoplastic polyurethane material in the same way as in ref. [25], so that the thick panels were rigid while the folds were elastic. The hollow fingertips were 3D-printed on a PolyJet printer (Stratasys-j735) using Agilus30 material, which came with a shore hardness of 30A to conform to objects. The fabrication parameters are in Table 5. The fingertips were securely affixed to the gripper backbone, with silicone sheets glued on top to increase surface friction. Clear nylon lines were used as tendons, which were arranged with the differential mechanism to finish the platform

**Table 5.** Fabrication parameters of the gripper (unit: mm).

$L$	$l$	$h$	$w_1$	$w_2$	$h_0$	$d_1$	$d_2$	$d_3$
45	10	10	1	1.2	0.3	2.8	4.3	3

as shown in Figure 5a. Two step motors (NEMA 17) were used to activate the tendon sets under the open-loop control of a microcontroller (Arduino UNO).

The gripper prototype could also be mounted on the robot arm (PANDA, Franka Emika) via a motor adapter, as shown in Figure 5b, where tendons could be pulled or loosened at the same time for simple grasping tasks under the control of one motor. Tubes were embedded into the fingers as illustrated in Figure 1b, connecting the pneumatic fingertips and the pressure sensor board (ADP5101) for data collection.

**Characterization of Basic Motion Modes:** To validate the motion modes shown in Figure 4, the gripper platform in Figure 5a was placed under a motion capture system (OptiTrack) to record the finger movements. Markers were attached at the finger ends. After calibration, the gripper was actuated to reach all possible motion modes. Closing and opening motions of the gripper were achieved by pulling and loosening relevant tendons. When both motors were needed, they were operated simultaneously. Each cycle was repeated five times, with an interval period of 5 s. The position data were recorded on software (Motive). The marker's size was taken into account to adjust Equation (7) and (8).

**Validation of Motion Switch at Non-Bifurcations:** Given the hinge compliance analysis, the gripper could complete transitions from one motion path to the other at non-bifurcations. According to Table 2, we selected the switch from motion types 2–4 or 5 to validate the hypothesis. The motor control strategy for types 2–4 was as follows. Each trial was repeated five times, at an interval of 5 s.

Step 1: When the gripper was unfolded,  $M_1$  rotated CW. The gripper moved to motion type 2.

Step 2:  $M_1$  was kept still.  $M_2$  rotated ACW to see whether the gripper could move to motion type 4.

Step 3:  $M_1$  and  $M_2$  returned to their original states, waiting until the gripper was flat.

The motor control to switch motion type 2 to 5 was the same, except that in the second step,  $M_2$  needed to rotate CW to see whether the gripper could move to motion type 5. In each motion switch, the fingers' positions were recorded.

**In-Hand Manipulation of Objects:** The gripper's capability for object manipulation was explored. To include basic geometric features of common objects, balls, cuboids, and cones were used to evaluate the gripper's function. The motor control strategy to manipulate each object was described as follows, the process of which is also illustrated in Figure 10 taking the ball as an example. Each trial was repeated five times and the interval time was 5 s. The movements of objects were recorded.

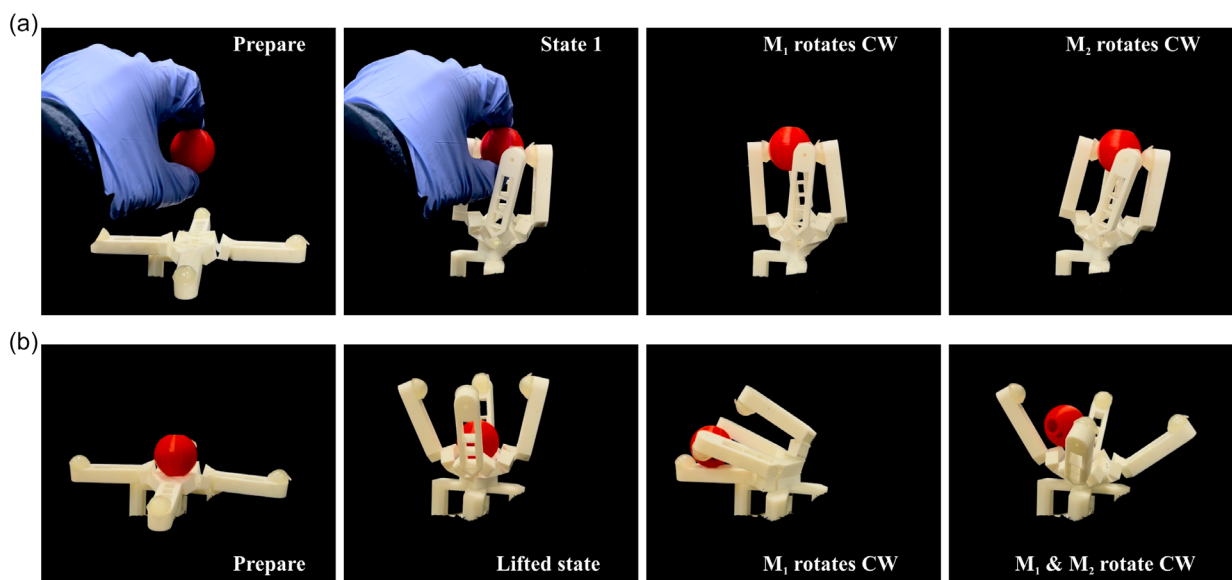


**Figure 10.** Key steps for ball manipulation by exploiting a) motion type 5 and b) combination of motion types 2 and 5.

The motor control for ball manipulation 1 as shown in Figure 10a:  
Step 1:  $M_1$  and  $M_2$  rotated CW synchronously.  
Step 2: The gripper moved into motion type 5 to grab a ball (state 1).  
Step 3:  $M_2$  stayed still.  $M_1$  continued CW rotation until it reached the maximum output torque.

Step 4:  $M_1$  returned to state 1 and was kept still. Likewise,  $M_2$  rotated CW until it reached the maximum output torque.

The motor control for ball manipulation 2 as shown in Figure 10b:  
Step 1: A ball was placed at the gripper center when it was unfolded.  
Step 2:  $M_1$  and  $M_2$  rotated CW synchronously.  
Step 3: The gripper moved into motion type 5 to lift the ball (lifted state).

Step 4:  $M_2$  released.  $M_1$  continued CW rotation to change the ball's position.

Step 5:  $M_1$  released until the gripper was flat.  $M_2$  rotated CW.  
Step 6: When the gripper was semi-folded, and  $M_1$  was also activated to rotate CW.

Step 7: The object was tracked and checked whether it could return to the lifted state.

The motor control for cuboid manipulation (similar to ball manipulation 1):

Step 1:  $M_1$  and  $M_2$  rotated ACW synchronously.  
Step 2: The gripper moved into motion type 3 to grab a cuboid (state 2).  
Step 3:  $M_2$  stayed still.  $M_1$  continued ACW rotation until it reached the maximum output torque.

Step 4:  $M_1$  returned to state 2 and was kept still. Likewise,  $M_2$  rotated ACW until it reached the maximum output torque.

The motor control for cone manipulation (also similar to ball manipulation 1):

Step 1:  $M_1$  rotated CW and  $M_2$  rotated ACW synchronously.  
Step 2: The gripper moved into motion type 4 to grab a cone (state 3).  
Step 3:  $M_2$  stayed still.  $M_1$  continued CW rotation until it reached the maximum output torque.

Step 4:  $M_1$  returned to the grasped state 3 and was kept still. Likewise,  $M_2$  rotated ACW until it reached the maximum output torque.

**Tactile Data Collection:** A series of grasping experiments were carried out on the gripper under motion type 5, where pneumatic sensors served as the gripper fingertips for tactile data collection. The setup is shown in Figure 5b. First, standardized objects of two sizes were used, whose bases were circle, square, hexagon, and triangle, as shown in Figure 9a. The grasp on each object was done until the motor reached its maximum output torque for at least 3 s. Each grasp was repeated three times and the pressure inside each fingertip was sampled at a frequency of 50 Hz. In addition to grasping standardized shapes, the gripper was also tested on a series of daily objects illustrated in Figure 9b. Similarly, the pressure on each fingertip was recorded for each grasp. A video of the experimental procedure is available in Section S2, Supporting Information.

## Supporting Information

Supporting Information is available from the Wiley Online Library or from the author.

## Acknowledgements

The help from Dr. Peter Walter and Dr. Oliver Shorthose is gratefully acknowledged. The authors would also like to thank the EPSRC Programme Grant "From Sensing to Collaboration" (EP/V000748/1) for making this research possible.

## Conflict of Interest

The authors declare no conflict of interest.

## Data Availability Statement

The data that support the findings of this study are available in the supplementary material of this article.

## Keywords

bifurcations, compliance, grippers, in-hand manipulation, kinematic analysis, thick-panel origami

Received: October 25, 2023

Revised: February 7, 2024

Published online: April 15, 2024

- [1] S. Cobos, M. Ferre, M. Sanchez Uran, J. Ortego, C. Pena, in *2008 IEEE/RSJ Int. Conf. on Intelligent Robots and Systems (IROS)*, IEEE, Nice, France, September 2008, pp. 2246–2251.
- [2] M. T. Mason, *Annu. Rev. Control Rob. Auton. Syst.* **2018**, 1, 1.
- [3] B. Zhang, Y. Xie, J. Zhou, K. Wang, Z. Zhang, *Comput. Electron. Agric.* **2020**, 177, 105694.
- [4] A. Billard, D. Kragic, *Science* **2019**, 364, eaat8414.
- [5] J. Ueda, M. Kondo, T. Ogasawara, *Mech. Mach. Theory* **2010**, 45, 224.
- [6] ShadowRobot, <https://www.shadowrobot.com/dexterous-hand-series/> (accessed: March 2024).
- [7] O. M. Andrychowicz, B. Baker, M. Chociej, R. Józefowicz, B. McGrew, J. Pachocki, A. Petron, M. Plappert, G. Powell, A. Ray, J. Schneider, S. Sidor, J. Tobin, P. Welinder, L. Weng, W. Zaremba, *Int. J. Rob. Res.* **2020**, 39, 3.
- [8] S. Puhlmann, J. Harris, O. Brock, *IEEE Trans. Rob.* **2022**, 38, 3434.
- [9] Ottobock, <https://www.ottobock.com/en-gb/product/8E70> (accessed: March 2024).
- [10] Ossur, <https://www.ossur.com/en-gb/prosthetics/arms/i-limb-quantum> (accessed: March 2024).
- [11] M. Catalano, G. Grioli, E. Farnioli, A. Serio, C. Piazza, A. Bicchi, *Int. J. Rob. Res.* **2014**, 33, 768.
- [12] B.-Y. Sun, X. Gong, J. Liang, W.-B. Chen, Z.-L. Xie, C. Liu, C.-H. Xiong, *IEEE Trans. Rob.* **2022**, 38, 2322.
- [13] M. Yim, W.-M. Shen, B. Salemi, D. Rus, M. Moll, H. Lipson, E. Klavins, G. S. Chirikjian, *IEEE Rob. Autom. Mag.* **2007**, 14, 43.
- [14] A. M. Dollar, R. D. Howe, in *Int. Symp. on Experimental Robotics*, Athens, Greece, July 2008.
- [15] N. Rojas, R. R. Ma, A. M. Dollar, *IEEE Trans. Rob.* **2016**, 32, 763.
- [16] K. M. Lynch, F. C. Park, *Modern Robotics*, Cambridge University Press, Cambridge, UK 2017.
- [17] R. L. Truby, M. Wehner, A. K. Grosskopf, D. M. Vogt, S. G. Uzel, R. J. Wood, J. A. Lewis, *Adv. Mater.* **2018**, 30, 1706383.
- [18] S. J. Yoon, M. Choi, B. Jeong, Y.-L. Park, *IEEE Trans. Rob.* **2022**, 38, 2179.
- [19] A. Pagoli, F. Chapelle, J. A. Corrales, Y. Mezouar, Y. Lapusta, *IEEE Rob. Autom. Lett.* **2021**, 6, 7706.
- [20] C. B. Teeple, R. C. St. Louis, M. A. Graule, R. J. Wood, in *2021 IEEE/RSJ Int. Conf. on Intelligent Robots and Systems (IROS)*, IEEE, Prague, Czech Republic, September 2021, pp. 7201–7208.
- [21] Q. Lu, N. Baron, A. B. Clark, N. Rojas, *Int. J. Rob. Res.* **2021**, 40, 1402.
- [22] J. Amend, H. Lipson, *Soft Rob.* **2017**, 4, 70.
- [23] D. Rus, M. Tolley, *Nat. Rev. Mater.* **2018**, 3, 101.
- [24] C. Liu, P. Maiolino, Y. Yang, Z. You, in *Int. Design Engineering Technical Conf. and Computers and Information in Engineering Conf.*, Vol. 83990, Online, American Society of Mechanical Engineers, August 2020, V010T10A080.
- [25] C. Liu, P. Maiolino, Z. You, *Front. Rob. AI* **2021**, 8, <https://doi.org/10.3389/frobt.2021.730227>.



- [26] L. Costi, P. Maiolino, F. Iida, *Front. Rob. AI* **2022**, 9, <https://doi.org/10.3389/frobt.2022.930405>.
- [27] O. Shorthose, A. Albin, L. Scimeca, L. He, P. Maiolino, in *2023 IEEE Int. Conf. on Soft Robotics (RoboSoft)*, IEEE, Singapore, April **2023**, pp. 1–7.
- [28] G. Mengaldo, F. Renda, S. L. Brunton, M. Bäcker, M. Calisti, C. Duriez, G. S. Chirikjian, C. Laschi, *Nat. Rev. Phys.* **2022**, 4, 595.
- [29] H. Hauser, R. M. Fuchsli, R. Pfeifer, <https://www.morphologicalcomputation.org/e-book#:~:text=E%2Dbook%20on%20Opinions%20and%20Outlook%20on%20Morphological%20Computation&text=The%20book%20is%20meant%20to,accessible%20for%20a%20broad%20audience> (accessed: March 2024).
- [30] C. Liu, Z. You, P. Maiolino, in *Int. Design Engineering Technical Conf. and Computers and Information in Engineering Conf.*, Vol. 86281, American Society of Mechanical Engineers, St Louis, USA, August **2022**, V007T07A062.
- [31] L. He, N. Herzig, T. Nanayakkara, P. Maiolino, *Soft Rob.* **2022**, 9, 1062.